EDDY CURRENT NONDESTRUCTIVE EVALUATION

Eddy current methods of nondestructive testing (NDT) (1,2) are one of the most commonly used methods for evaluating the integrity of materials in industry. Although there are several different eddy current methods, they all rely on the principles of electromagnetic induction to ascertain the condition of a given test specimen. The basic principle underlying such methods can be illustrated with a simple arrangement shown in Fig. 1.

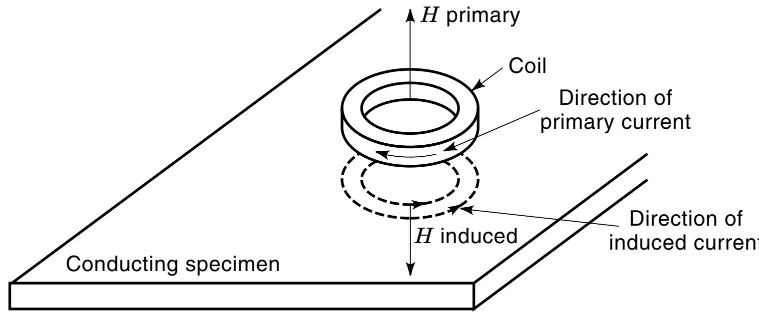

Figure 1. Eddy current probe over a conducting test specimen.

Consider a coil placed over an electrically conducting, nonferromagnetic test specimen. If the coil is excited by an alternating-current source, an alternating magnetic field is established. The alternating magnetic field causes currents to be induced in the conducting test specimen in accordance with the Maxwell–Faraday law. The induced currents are called eddy currents since they follow closed circulatory patterns that are similar to eddies found in bodies of water. The alternating eddy current, in turn, establishes a field whose direction is opposite to that of the original or primary field. Consequently, the net flux linkages associated with the coil decreases. Since the inductance of a coil is defined as the number of flux linkages per ampere, the effective inductance of the coil decreases relative to its value if it were to be suspended in air. The presence of eddy currents in the test specimen also results in a resistive power loss. The effect of this power loss manifests in the form of a small increase in the effective resistance of the coil. An exaggerated view of the changes in the terminal characteristics of the coil is shown in Fig. 2, where the variation in resistance and inductance is plotted in the impedance plane. When a flaw or inhomogeneity whose conductivity differs from that of the host specimen is present, the current distribution is altered. Consequently, the impedance of the coil changes relative to its value obtained with an unflawed specimen, as shown in Fig. 2. A system that is capable of monitoring the changes in impedance can, therefore, be used to detect flaws in a specimen that is scanned by a coil. It is not necessary to rely on impedance measurements to detect the presence of flaws. Systems that rely on the measurement of the coil currents and voltages have also been used for detecting flaws. A more detailed discussion relating to variations of the method as well as some simple transducer configurations follows after a brief introduction to the underlying theory.

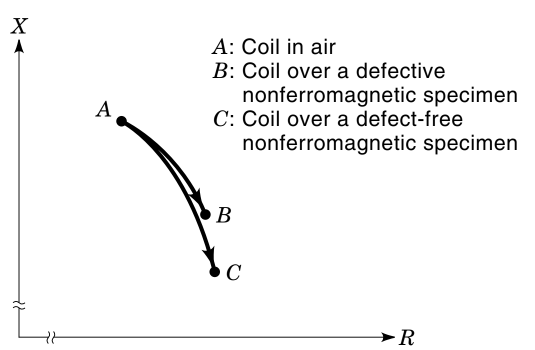

Figure 2. Exaggerated view of the impedance-plane trajectory of a coil over a conducting nonferromagnetic test specimen.

MATHEMATICAL MODEL

The eddy current nondestructive evaluation phenomena, in common with all electromagnetic phenomena, are governed by Maxwell's equations (3). Three of these equations that are pertinent to eddy current testing are

$$\nabla \times \boldsymbol{E} = -\frac{\partial \boldsymbol{B}}{\partial t} \tag{1}$$

$$\nabla \times \boldsymbol{H} = \boldsymbol{J} + \frac{\partial \boldsymbol{D}}{\partial t} \tag{2}$$

$$\nabla \cdot \boldsymbol{B} = 0 \tag{3}$$

where $\boldsymbol{E}$ is the electric field intensity (V/m), $\boldsymbol{H}$ is the magnetic field intensity (A/m), $\boldsymbol{B}$ is the magnetic flux density (Wb/m^2) and J is the current density (A/m^2). The coil excitation frequencies are typically very low (<10 MHz) and consequently the displacement current term ($\partial\boldsymbol{D}/\partial t$) in Eq. (2) can be neglected. Equation (2), therefore, reduces to

$$\nabla \times \boldsymbol{H} = \boldsymbol{J} \tag{4}$$

Since $\boldsymbol{B}$ is divergence free, it can be expressed as

$$\boldsymbol{B} = \nabla \times \boldsymbol{A} \tag{5}$$

where $\boldsymbol{A}$ is called the vector magnetic potential. Substituting Eq. (5) in Eq. (1) and using Eq. (4) as well as the constitutive relationships $\boldsymbol{B} = \mu\boldsymbol{H}$ and $\boldsymbol{J} = \sigma\boldsymbol{E}$, the following result can be derived:

$$\nabla \times \frac{1}{\mu}\nabla \times \boldsymbol{A} = \boldsymbol{J}_s + \sigma\frac{\partial \boldsymbol{A}}{\partial t} \tag{6}$$

where $\boldsymbol{J}_s$ is the applied or impressed current density. Equation (6) is a parabolic partial differential equation that governs the physical process underlying eddy current phenomena and is applicable for situations involving both sinusoidal as well as nonsinusoidal excitation. If the coil is excited by a sinusoidal source, then, the governing equation can be simplified, assuming steady state conditions to the elliptic equation,

$$\nabla \times \left(\frac{1}{\mu}\nabla \times \boldsymbol{A}\right) = \boldsymbol{J}_s - j\omega\sigma\boldsymbol{A} \tag{7}$$

where $\omega = 2\pi f$ is the angular excitation frequency (rad/s) and $j = \sqrt{-1}$. The partial differential equation represented by Eqs. (6) or (7) can be solved with appropriate boundary conditions to obtain the vector magnetic potential A in the region of interest.

Other measurement quantities of interest, such as the coil impedance Z, induced coil voltage V_i, and eddy current density J_e can be derived using

$$Z = \left(\frac{j\omega}{\boldsymbol{I}_s}\right) \int_c \boldsymbol{A} \cdot d\boldsymbol{l} \tag{8}$$

$$V_i = (j\omega) \int_c \boldsymbol{A} \cdot d\boldsymbol{l} \tag{9}$$

$$\boldsymbol{J}_e = -j\omega\sigma\boldsymbol{A} \tag{10}$$

The solution of the underlying partial differential equation is fraught with several challenges due to the awkward boundary conditions. Analytical as well as numerical approaches to addressing the problem are discussed in a later section.

The electromagnetic field decays exponentially as a function of depth within the test specimen. Eddy current methods, as a general rule, are not very effective for detecting defects that lie deep in the material. The rate of decay is a function of the excitation frequency f, as well as the conductivity and permeability of the test specimen. A useful index that is often employed in industry is called the skin depth. The skin depth δ is defined as the depth at which the eddy current decays to $1/e$ or 36.8% of the value at the surface. If an infinite sheet of current is induced at the surface of a conducting half-plane, the current decays to $1/e$ of the value at the surface, at a depth δ given by

$$\delta = \frac{1}{(\pi f \mu \sigma)^{1/2}} \tag{11}$$

Although the value of the skin depth as given by Eq. (11) is applicable for the theoretical case of a half-plane specimen, it is nevertheless often used as a guide for choosing the excitation frequency for a given test specimen. Lower excitation frequencies have to be employed for detecting flaws that are located deep in the specimen. Likewise, the skin depth "rule" dictates that, other factors being equal, lower excitation frequencies have to be used when the specimen conductivity is high.

Eddy Current Probes

A variety of eddy current probes are in use today, and a full discussion relating to their type and characteristics is beyond the scope of this short article. The eddy current probe described in the introductory section is an absolute probe. In practice the change in the impedance of the coil due to a defect is very small relative to its quiescent value. The challenges associated with the measurement of these small perturbations in the presence of variations contributed by changes in the environment (temperature, noise, etc.) can be formidable. Differential probes (1,4) are often used to overcome some of these problems. Figure 3 shows a simple differential eddy current probe that is used for inspecting tubes. The probe consists of two identical coils that are spaced apart by a small distance. Consider a situation in which the probe is moved past a small defect such as a crack. When the probe is positioned in a defect-free region of the tube, the impedances of the two coils are identical. Consequently the differential impedance is zero. As the leading coil moves past the defect, the change in its impedance causes the differential impedance to trace one of the lobes (lobe A) shown in Fig. 3. When the defect lies between the two coils, the impedances of the both coils are equal and hence the differential impedance is zero. When the trailing coil moves past the defect the second lobe (B) in the impedance plane trajectory is traced. After the trailing coil has moved past the defect, the differential impedance reduces to zero. The shape of the impedance plane trajectory is a function of the shape of the defect, excitation frequency, and probe design. Defect characterization usually involves analysis of the impedance plane trajectory. The differential nature of the probe makes it relatively insensitive to effects of temperature and variations in the spacing between the specimen and the probe (often called the lift-off). The probe is also, unfortunately, less sensitive to long axial cracks. Several variations of the basic design have been proposed in recent years to overcome this deficiency. Commercial absolute probes often use a differential arrangement in which the reference coil is located away from the specimen. The difference in the impedances of the two coils is measured.

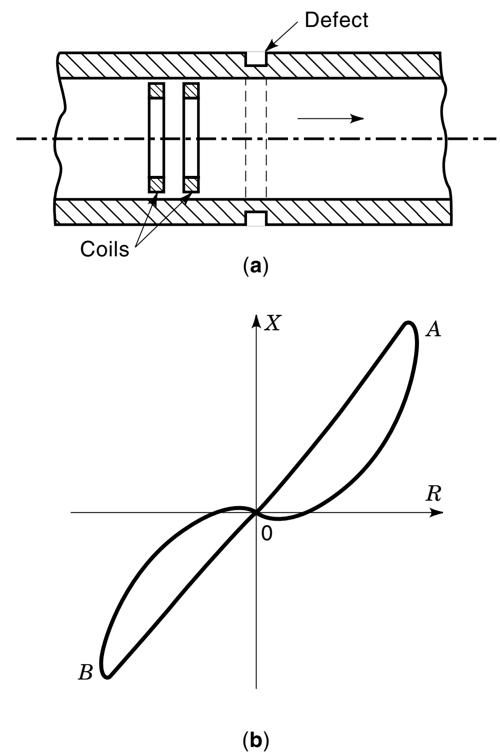

Figure 3. (a) Differential eddy current probe used for inspecting tubes; (b) Impedance-plane trajectory traced for an OD slot on the tube.

The electromagnetic "footprint" of most eddy current probes is large. This contributes to poor resolution and the need for using deconvolution procedures. One of the most

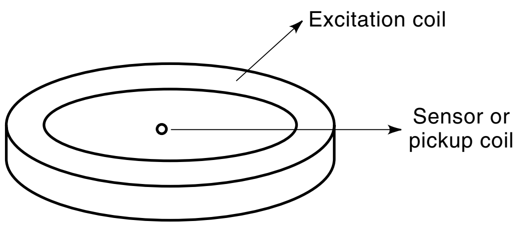

Figure 4. High-resolution eddy current probe.

commonly used techniques is to employ a ferrite core with a small tip to improve resolution. The ferrite core concentrates the field, thereby improving the resolution. Other methods include the use of copper shielding (4) as well as active compensation methods (through the use of auxiliary coils) (5). Figure 4 shows an alternative approach involving the use of a large excitation coil combined with a very small sensor or pickup coil. The small size of the sensor coil improves the resolution. Other probe designs include those that rely on the establishment of a uniform field and the detection of small perturbations in the field. Nuclear utilities also employ probes that rotate for inspecting tubes (4).

A number of new field sensors have emerged in recent years. High-sensitivity Hall sensors and magnetodiodes as well as self-contained sensors that include amplifiers and temperature compensation circuits are increasingly being used as sensors instead of coils. Another exciting development is related to the availability of relatively low-cost superconducting quantum interference devices (SQUIDS) (6), which are capable of measuring extremely low fields. Several researchers are investigating the feasibility of using such sensors for detecting extremely small and deeply embedded defects.

EDDY CURRENT TECHNIQUES

The test setup used in the introductory section to explain the concept of eddy current testing involved the use of a single coil excited by an alternating current source. Several variations of this basic scheme are used in industry.

A simple extension of the concept is to employ multiple excitation frequencies to exploit the fact that the depth of penetration is a function of the excitation frequency. Defects and artifacts that are close to the surface can be detected with greater levels of sensitivity using high-frequency excitation signals. Low excitation frequencies can be used to detect defects that lie in the recesses of the material. The responses obtained at the two excitation frequencies can be combined appropriately to suppress contributions selectively from extraneous artifacts that are present in the vicinity of the defect and prevent direct observation of the defect signal. The excitation signals can be applied to the eddy coil either sequentially in a time division or simultaneously in a frequency-division multiplexed manner.

As an example, multifrequency methods are used extensively in nuclear utilities for extracting defect signals that are masked by unwanted signals from artifacts such as support plates. Consider a case where a small defect exists in a tube, which is anchored and held in place by a support plate as shown in Fig. 5. If the tube is inspected using a differential eddy current probe, the signals due to the defect and the support plate would overlap, particularly if the flaw were to be close to the plate. This is evident from Fig. 6(a), which shows a composite impedance-plane trajectory. The defect signal is clearly corrupted by the larger support-plate signal. Multifrequency methods involve measurement of the eddy current signal at two different excitation frequencies. The first signal is captured using a high excitation frequency so as to obtain a response that is relatively more sensitive to the defect. The second signal is captured using a low excitation frequency to obtain a relatively high level of sensitivity to the support plate. Figures 6(a) and 6(b) represent impedance-plane trajectories obtained at high and low excitation frequencies, respectively. The two signals are then “mixed” to suppress the support-plate signal. Mixing is performed by first transforming (rotating, scaling, and translating) the second impedance-plane trajectory. The transformation parameters are chosen such that the transformed and the second impedance-plane trajectory are as similar as possible to each other. The transformed signal is subtracted from the first signal to obtain the defect signal. Figure 6(c) shows the result of mixing the signals shown in Figs. 6(a) and 6(b). The mixing can be accomplished either manually or automatically (7,8) by estimating the transformation parameters in a manner that minimizes an appropriate cost function. The cost function could, for example, be the energy in the error between the transformed and first impedance-plane trajectories. This example shows how a pair of eddy current signals obtained at two different excitation frequencies can be “mixed” to suppress indications from unwanted artifacts. The concept can be easily extended for mixing more than two signals for suppressing one or more artifact indications.

Skin-effect considerations limit the use of conventional eddy current methods to the detection of either surface breaking or shallow defects. Inner-diameter (ID) eddy current

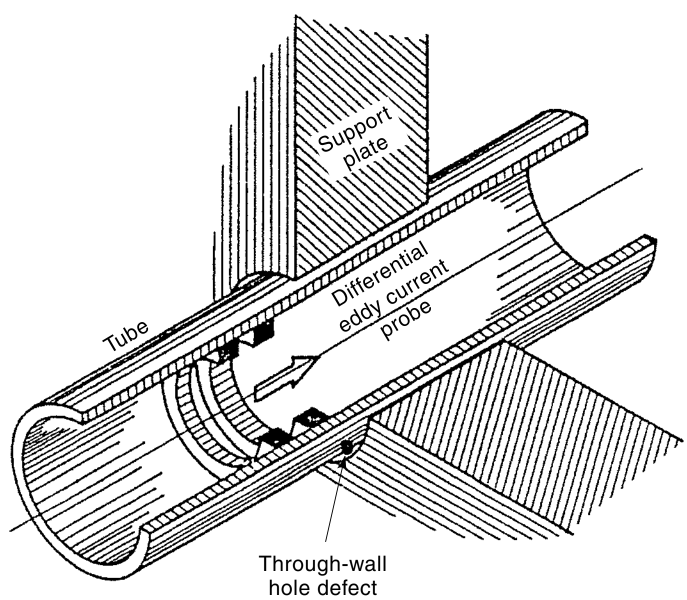

Figure 5. Differential eddy current within a tube and moved by a ferromagnetic support plate. The tube contains a defect near the support plate.

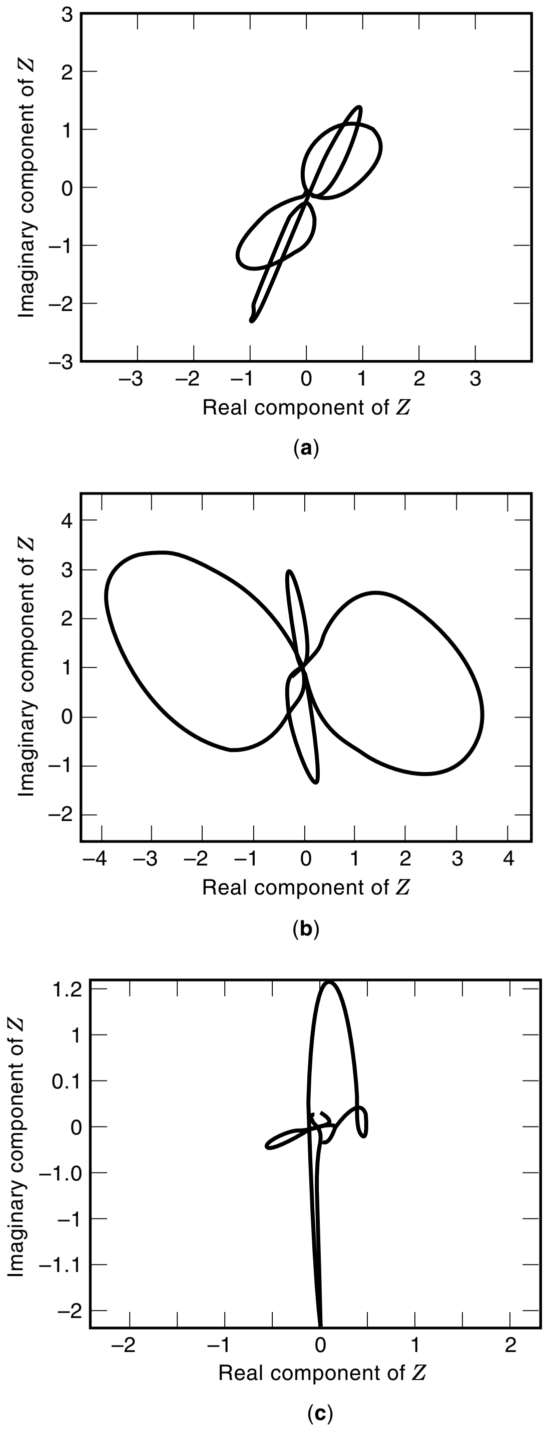

Figure 6. (a) Composite impedance-plane trajectory obtained at 400 kHz excitation frequency; (b) Composite impedance-plane trajectory obtained at 200 kHz; (c) Signal obtained after mixing signals shown in (a) and (b).

probes, for example, are more sensitive to defects that lie on the inner surface of thick-walled tubes. Special techniques that increase the level of penetration or alternatively the use of high-sensitivity sensors such as SQUIDs are required if ID probes are to be used. Recent years have witnessed the growth in popularity of a new technique that exploits the remote-field eddy current phenomenon (9,10). A major advantage lies in the sensitivity of the technique to inner- as well as outer-diameter (OD) defects. Figure 7 shows a typical remote-field eddy current probe used for the inspection of pipes. An excitation coil that is energized by a relatively low-frequency ac source establishes the eddy current field. Remote-field eddy current methods employ measurements taken at a distance from the excitation coil, unlike conventional methods that rely on field measurements in the vicinity of the excitation coil. The sensor coil is typically located two to three pipe diameters way from the excitation coil along the axis of the pipe. The eddy current field distribution can be divided into three regions. The field in the vicinity of the excitation coil (region 1) follows intuition in that the field magnitude decays exponentially with increasing radial distance from ID to OD. In the remote region (region 3), which occurs at a distance two to four pipe diameters away from the excitation coil along the axis of the pipe, the field magnitude decays from the OD to ID. This is in complete contrast to the behavior of the field in the vicinity of the excitation coil. The field distribution in the transition zone between these two regions (region 2) is characterized by very rapid changes. Energy that is directed outward, away from the excitation coil, interacts with the energy that travels close to the outer surface before traveling inward. The interaction causes the eddy current and vector magnetic potential magnitudes to drop to zero (potential valleys) at points in the pipe wall. Similarly, the phase of the eddy current undergoes rapid transitions (phase knots) in the pipe wall. Figure 8 shows the energy-flow pattern in the pipewall. The phenomenon is interesting in that it is characterized by a process wherein the field levels decay both from ID to OD (region 1) as well as from OD to ID (region 3). This renders the method sensitive to both ID as well as OD flaws in contrast to conventional eddy current methods that are sensitive to ID flaws only (for an ID probe).

Unlike conventional eddy current methods, the remote-field methods typically involve the measurement of the phase difference between the excitation signal and the voltage induced in the sensor coil. A lock-in amplifier is typically used since the field values in the remote and transition regions are very low and measurement is difficult due to poor signal-to-noise ratios.

The remote-field eddy current methods are used largely for the inspection of ferromagnetic tubes. Extensions of the method for the inspection of nonferromagnetic pipes as well as flat sheets and plates have been proposed in recent years. The industry has been quick to exploit the phenomena and many commercial systems are now available.

Multifrequency methods use two or more excitation frequencies to exploit the skin-effect phenomenon and to

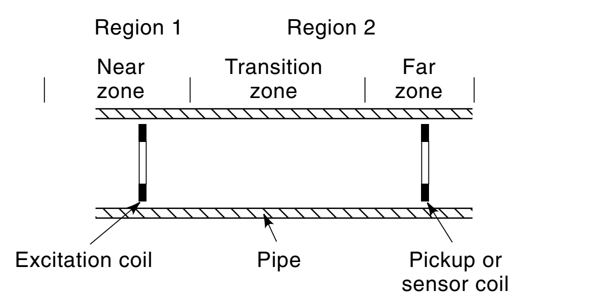

Figure 7. Typical remote-field eddy current probe arrangement.

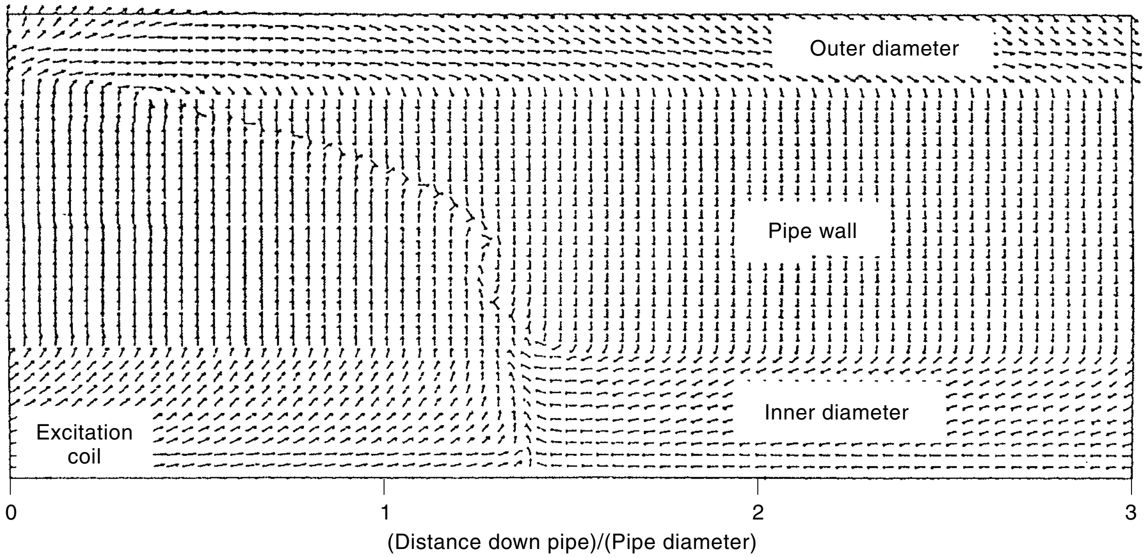

Figure 8. Energy-flow pattern in the pipewall.

heighten selectively the flaw detection sensitivity at various depths. An alternative is to use a spectrally rich signal such as a pulse to excite the probe (11). Figure 9 shows a typical setup using a pulsed eddy current to inspect spot welds. A relatively high-energy pulse energizes the excitation coil. The energy diffuses through the material and induces a signal in the sensor coil. The sensor coil signal is analyzed to ascertain the condition of the test specimen. Pulsed eddy current methods are used for characterizing thin films, spot welds, and a host of other applications.

Instrumentation. The instrumentation used is simple and straightforward. Figure 10 shows a block diagram of a typical eddyscope. The excitation coil is energized by a variable frequency sinusoidal current source. If the impedance of the coil is $Z\underline{/\theta}$ then the voltage across the coil is

$$V = I|Z|\cos(2\pi f_c t + \theta) \tag{12}$$

where f_c is the excitation frequency (Hz), $\theta = \tan^{-1}(2\pi f_c L/R)$ (rad), L is the effective inductance of the coil (H), and R is the effective resistance of the coil (Ω). The signal V is amplified using a low-noise, wideband amplifier.

The real component of the eddy current probe impedance is obtained by demodulating the amplified signal with the inphase output ($A \cos 2\pi f_c t$) of the variable-frequency oscillator and low-pass filtering the result. The output of the demodulator is

$$\begin{aligned} V_p &= k\cos(2\pi f_c t + \theta)\cos(2\pi f_c t) \\ &= \frac{k}{2}[\cos(4\pi f_c t + \theta) + \cos(\theta)] \end{aligned} \tag{13}$$

where k is related to the magnitude of the eddy current probe impedance Z. The high-frequency component is filtered by a low-pass filter. The output of the low-pass filter is

$$V_r = C_1|Z|\cos(\theta) \tag{14}$$

where C_1 is a constant.

Similarly, the imaginary component of the eddy current probe impedance is obtained by demodulating the amplified signal with the quadrature output ($A \sin 2\pi f_c t$) of the oscillator and low-pass filtering the output. The output of the demodulator is

$$\begin{aligned} V_q &= k\cos(2\pi f_c t + \theta)\sin(2\pi f_c t) \\ &= \frac{k}{2}[\sin(4\pi f_c t + \theta) + \sin(\theta)] \end{aligned} \tag{15}$$

The output of the low-pass filter is

$$V_i = C_2|Z|\sin\theta \tag{16}$$

where C_2 is a constant. V_r and V_i are outputs that are related to the real and imaginary components of the probe impedance. Most commercial instruments allow the signals to be sampled, digitized, and stored in memory. Eddyscopes also offer a feature that permits the impedance-plane trajectories to be rotated through an arbitrary angle θ_r. The output of the rotator is given by

$$x = V_r\cos\theta_r - V_i\sin\theta_r \tag{17}$$

$$y = V_i\cos\theta_r + V_r\sin\theta_r \tag{18}$$

The rotation feature allows the user to rotate the signal and ensure that signal changes due to lift-off (distance between

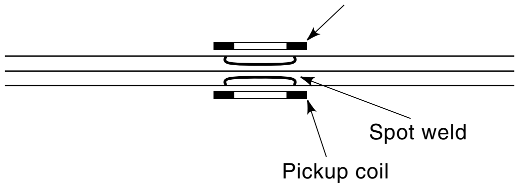

Figure 9. Typical pulsed eddy current probe setup for inspecting spot welds.

the probe and the test specimen) variations result in a trajectory that is either along the real or imaginary axis. After the rotation angle is adjusted, subsequent measurements are projected along the other axis to obtain relative immunity to the effects of lift-off.

Most eddyscopes are either housed in or interfaced to a personal computer. Highly sophisticated signal-processing algorithms can be implemented on the computer to analyze the signals.

Multifrequency eddy current instruments are similar to single-frequency instruments except that it is possible to apply two or more excitation signals to the eddy current coil either simultaneously or in a time-multiplexed mode. If the excitation signals are applied in a time-multiplexed mode, an appropriate time-windowing scheme is employed to separate the individual eddy current responses at each excitation frequency. If the excitation signals are applied simultaneously, classical frequency-division demultiplexing methods can be used to isolate the individual eddy current responses (12).

FORWARD PROBLEM MODELING

Computational eddy current models are extremely valuable in providing a visualization of the field distribution around the probe coil and the test sample. Such capabilities help not only in understanding the physics of the underlying process but also in optimization of probe design as well as the development of defect characterization schemes for mapping measured eddy current signals onto defect profiles. Eddy current models developed to date fall broadly into two main classes, namely, analytical and numerical.

Analytical Models

One of the earliest analytical results for the eddy current phenomenon was obtained by Dodd and Deeds (13). The governing equation in terms of the vector magnetic potential $\boldsymbol{A}$ for a linear isotropic, homogeneous media due to applied current density $\boldsymbol{J}_s$ is

$$\nabla^2 \boldsymbol{A} = -\mu \boldsymbol{J}_s + \mu\sigma \frac{\partial \boldsymbol{A}}{\partial t} \tag{19}$$

In the case of an axisymmetric geometry with only the φ component of $\boldsymbol{J}$ and $\boldsymbol{A}$, and a sinusoidal excitation, the equation in cylindrical coordinates is

$$\frac{\partial^2 \boldsymbol{A}}{\partial r^2} + \frac{1}{r}\frac{\partial \boldsymbol{A}}{\partial r} + \frac{\partial^2 \boldsymbol{A}}{\partial z^2} - \frac{\boldsymbol{A}}{r^2} = -\mu \boldsymbol{J}_s + j\omega\mu\sigma \boldsymbol{A} \tag{20}$$

Assuming the probe to be a δ-function coil at (r_0, z_0), the equation becomes

$$\frac{\partial^2 A}{\partial r^2} + \frac{1}{r}\left(\frac{\partial A}{\partial r}\right) + \frac{\partial^2 A}{\partial z^2} - \frac{A}{r^2} - j\omega\mu\sigma A = \mu J_s \delta(r - r_0)\delta(z - z_0) \tag{21}$$

This equation is solved using the separation of variables method for a coil over a planar conductor or a coil inside a cylindrical tube as shown in Fig. 3(a). The solution for both geometries are given in terms of integrals of Bessel functions. The vector potential due to other coil configurations is then obtained using the superposition principle.

In an attempt to establish a more quantitative interpretation of the eddy current response, Auld et al. (14) formulated a mathematical flaw response model for rectangular surface-breaking defects based on the Lorentz reciprocity relation

$$\boldsymbol{\nabla} \cdot (\boldsymbol{E}' \times \boldsymbol{H} - \boldsymbol{E} \times \boldsymbol{H}') = \boldsymbol{0} \tag{22}$$

where $\boldsymbol{E}$, $\boldsymbol{H}$ and $\boldsymbol{E}'$, $\boldsymbol{H}'$ are solutions of Maxwell's equations, at any point in the presence and absence of the flaw, respectively.

A third approach for obtaining an analytical solution proposed by Sabbagh et al. (15) uses the volume integral formulation. Based on an algorithm used for simulating the electromagnetic responses of three-dimensional bodies in layered

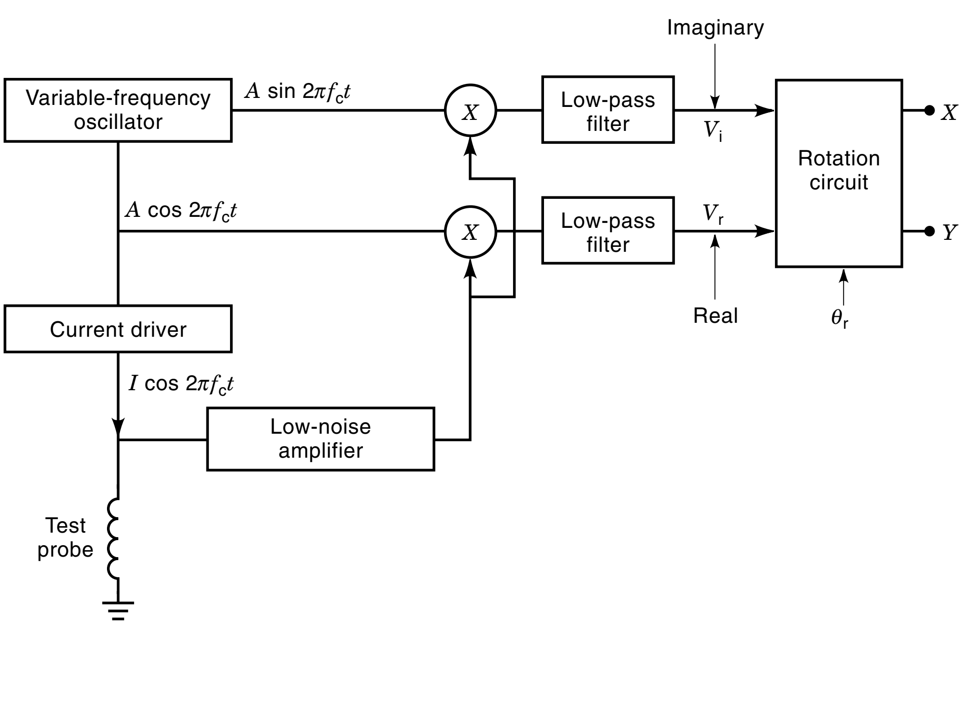

Figure 10. Block diagram of a single-frequency eddyscope.

media (16), Sabbagh et al. developed an eddy current NDT model where the inhomogeneities in a conducting specimen are replaced by an equivalent current distribution approximated by pulse basis functions. The current source representing the flaw produces a perturbation field at the probe coil that is then responsible for the eddy current signal. The change in probe impedance due to a flaw is defined as

$$\Delta z = \frac{\text{(emf induced by the perturbed field at the coil)}}{\text{(excitation current)}} \tag{23}$$

The conductivity $\sigma_0(\boldsymbol{r})$ of the test material is expressed as $\sigma_0(\boldsymbol{r}) = \sigma_f(\boldsymbol{r}) + \delta\sigma_0(\boldsymbol{r})$, where $\sigma_f(\boldsymbol{r})$ is the conductivity of a flaw and $\delta\sigma_0(\boldsymbol{r})$ is the perturbation in conductivity

$$\delta\sigma_0(\boldsymbol{r}) = \begin{cases} 0 & \text{outside the defect} \\ \sigma_f(\boldsymbol{r}) - \sigma_0(\boldsymbol{r}) & \text{inside the defect} \end{cases} \tag{24}$$

Substituting this conductivity function into the diffusion equation for $\boldsymbol{E}$, we see that the discontinuity in conductivity introduces a perturbation source term in the equation as

$$\boldsymbol{J}_f = [\sigma_f(\boldsymbol{r}) - \sigma_0(\boldsymbol{r})]\boldsymbol{E}(\boldsymbol{r}) \tag{25}$$

$$\nabla^2\boldsymbol{E} - j\omega\mu\sigma_0\boldsymbol{E} = j\omega\mu\boldsymbol{J}_0 + j\omega\mu[\sigma_f(\boldsymbol{r}) - \sigma_0(\boldsymbol{r})]\boldsymbol{E} \tag{26}$$

The implementation of this method for the axisymmetric geometry consisting of an excitation and pickup coil pair moving in the interior of a tube consists of the following steps.

1. Compute the Green's function for the desired positions of the source. For the given geometry, $G_{ij}(\boldsymbol{r}, \boldsymbol{r}')$ corresponds to a field at $\boldsymbol{r}$ in region i due to a filamentary coil at $\boldsymbol{r}'$ in region j. The regions are labeled as 1, tube interior; 2, tube wall; 3, tube exterior.
2. Calculate the unperturbed field for the defect-free medium as

$$\boldsymbol{E}_0(\boldsymbol{r}) = \int_{\text{coil}} G(\boldsymbol{r}, \boldsymbol{r}') J_0(\boldsymbol{r}')\, dv' \tag{27}$$

3. Calculate the equivalent current source $J_f(\boldsymbol{r})$ for the flaw by solving

$$\boldsymbol{E}_f(\boldsymbol{r}) = \boldsymbol{E}_0(\boldsymbol{r}) + \int_{\text{flaw}} G_{12}(\boldsymbol{r}, \boldsymbol{r}')[\sigma_f(\boldsymbol{r}) - \sigma_0(\boldsymbol{r}')]\boldsymbol{E}_f(\boldsymbol{r}')\, dv' \tag{28}$$

4. Compute the perturbation field at the coil using the current source from step 3:

$$\boldsymbol{E}_f(\boldsymbol{r}) = \boldsymbol{E}_0(\boldsymbol{r})|_{\text{coil}} = \int_{\text{flaw}} G_{12}(\boldsymbol{r}, \boldsymbol{r}') J_f(\boldsymbol{r}')\, dv' \tag{29}$$

5. Compute the emf induced in the coil using

$$\text{emf} = n \int_{\text{coil}} \boldsymbol{E}_f(\boldsymbol{r}) \cdot \boldsymbol{dl} \tag{30}$$

The eddy current probe impedance is then calculated using $Z = \text{emf}/I$.

Numerical Models

Analytical models are desirable because they provide exact closed-form solutions that provide a functional relation between experimental parameters and the measured eddy current signal. However, the relative complexity of such methods and their limitations in terms of their inability to deal with nonlinearities and the restricted classes of problem geometries that can be handled have limited their usefulness. In contrast, numerical solutions are not limited by geometrical complexities or material nonlinearities. The high-speed computational power and storage capabilities of modern-day computers have led to the extensive development and use of numerical techniques for solving and simulating a wide variety of physical situations. The principal numerical methods that are in use in electromagnetic NDT are the finite-difference, finite-element, and hybrid techniques such as boundary-element methods.

Finite-Difference Formulation. The finite-difference method is based on replacing domains and differential operators by a discrete grid of nodes and difference quotients, respectively. Once the difference equations are obtained, the task of solving the problem numerically consists of writing the difference equations for each nodal point in the grid in terms of the values at the appropriate neighboring nodes. This results in a set of linear algebraic equations written in a matrix form. The matrix of coefficients is then inverted to obtain the unknown fields at the nodal points.

Dodd (17) solved the complete, nonlinear eddy current problem for the inhomogeneous material case using finite-difference operators. For axisymmetric geometries such as a coil above a conducting plane or a coil encircling a tube with sinusoidal excitation, the equation can be written as

$$\begin{aligned} &\frac{\partial^2 A}{\partial r^2} + \frac{1}{r}\frac{\partial A}{\partial r} + \frac{\partial^2 A}{\partial z^2} - \frac{A}{r^2} \\ &= -\mu J_s + j\omega\mu\sigma A - \mu\left[\frac{\partial}{\partial r}\left(\frac{1}{\mu}\right)\left(\frac{1}{r}\frac{\partial rA}{\partial r}\right) + \frac{\partial}{\partial z}\left(\frac{1}{\mu}\right)\frac{\partial A}{\partial z}\right] \end{aligned} \tag{31}$$

Using central difference operators for all differentiations except for permeability variations across interface boundaries where forward difference operators are used, the vector potential at a point (r, z) in terms of four nearest neighbors is

$$\begin{aligned} A_{r,z} = &\left(\frac{1+a}{r}\frac{\mu_{r,z}}{\mu_{r+a,z}}A_{r+a,z} + A_{r-a,z} + \frac{\mu_{r,z}}{\mu_{r,z+a}}A_{r,z+a}\right. \\ &\left. + A_{r,z-a} + a^2\mu_{r,z}J_{r,z}\right) \\ &+ \left(z + \frac{a}{r} + \frac{a^2}{r^2} + \frac{\mu_{r,z}}{\mu_{r+a,z}} + \frac{\mu_{r,z}}{\mu_{r,z+a}} + ja^2\omega\mu_{r,z}\sigma_{r,z}\right) \end{aligned} \tag{32}$$

where $\mu_{r,z}$, $J_{r,z}$, and $\sigma_{r,z}$ have specified values at each nodal point in the two-dimensional rectangular grid. The nonlinearities associated with medium permeability are also incorporated in the formulation without additional computations.

The major disadvantage of the finite-difference method (17) is one of fitting a regular grid to geometries that have curved boundaries and interfaces. One has to resort to using a mixture of rectangular and cylindrical coordinates, resulting in added complexity of programming and implementation. Also, increasing the mesh density to satisfy the boundary requirements may result in a large grid size and computer requirements without contributing to the accuracy of the final solution.

Finite-Element Formulation. A more widely used numerical model employs finite-element (FE) analysis techniques and has its origin in the fields of solid mechanics, structural analysis, and heat transfer. Finite-element analysis techniques was first applied by Chari to electromagnetics (18) for studying the eddy current problem in magnetic structures and later by Brauer (19) for determining induced fields and currents in transformers. The modeling technique was then used extensively by Lord and associates for the investigation of various problems in electromagnetic NDT. Palanisamy and Lord (20,21) developed a two-dimensional axisymmetric finite-element model for predicting eddy current probe signals from defects in steam generator tubing. Ida (22) developed a three-dimensional finite-element model for eddy current nondestructive evaluation applications.

The finite-element technique is based on principles of variational calculus (23) in which the solution of a differential equation is obtained as the stationary value of a functional. In eddy current problems, the functional represents the energy of the system so that the stationary value is a minimum. The principles of variational calculus can be used to show that the differential equation is satisfied by a function that simultaneously minimizes the appropriate energy functional (24). A brief description of the finite-element formulation for an axisymmetric geometry of a differential coil probe inside a tube follows.

Assuming a linear, isotropic, and homogeneous medium and a sinusoidal excitation source, the governing diffusion Eq. (20) is

$$\frac{1}{\mu}\left(\frac{\partial^2 \boldsymbol{A}}{\partial r^2}+\frac{1}{r}\frac{\partial \boldsymbol{A}}{\partial r}+\frac{\partial^2 \boldsymbol{A}}{\partial z^2}-\frac{\boldsymbol{A}}{r^2}\right)=j\omega\sigma\boldsymbol{A}-\boldsymbol{J}_{\mathrm{s}} \tag{33}$$

The corresponding energy functional obtained from variational principles is

$$F=\iint_R\left[\frac{1}{2\mu}\left(\left|\frac{\partial \boldsymbol{A}}{\partial r}+\frac{\boldsymbol{A}}{r}\right|^2+\left|\frac{\partial \boldsymbol{A}}{\partial z}\right|^2\right)+\frac{j\omega\sigma}{2}|\boldsymbol{A}|^2-\boldsymbol{J}_{\mathrm{s}}\times\boldsymbol{A}\right]r\,dr\,dz \tag{34}$$

The terms in Eq. (34) can be recognized as the energy terms due to the magnetic field, eddy currents, and the input source.

The region of interest is discretized using a mesh consisting of triangular elements connected to each other at the nodes. A sample FE mesh for the axisymmetric geometry in Fig. 3 is shown in Fig. 11. Using linear or higher-order interpolation functions $[N]$ to express the magnetic vector potential $\boldsymbol{A}$ at any point within an element, the energy functional for an element can be written in terms of its unknown nodal values A_i, A_j, A_k as

$$F_{\mathrm{e}}=\int_v\frac{1}{2}\left[\frac{1}{\mu}\left(\frac{\partial N}{\partial y}\right)^2+\frac{1}{\mu}\left(\frac{\partial N}{\partial x}\right)^2-2J[N]\right]\begin{bmatrix}A_i\\A_j\\A_k\end{bmatrix} \tag{35}$$

Minimizing F_{e} with respect to the nodal point values gives a set of linear algebraic equations

$$\frac{\partial F_{\mathrm{e}}}{\partial A_l}=0,\qquad l=i,j,k \tag{36}$$

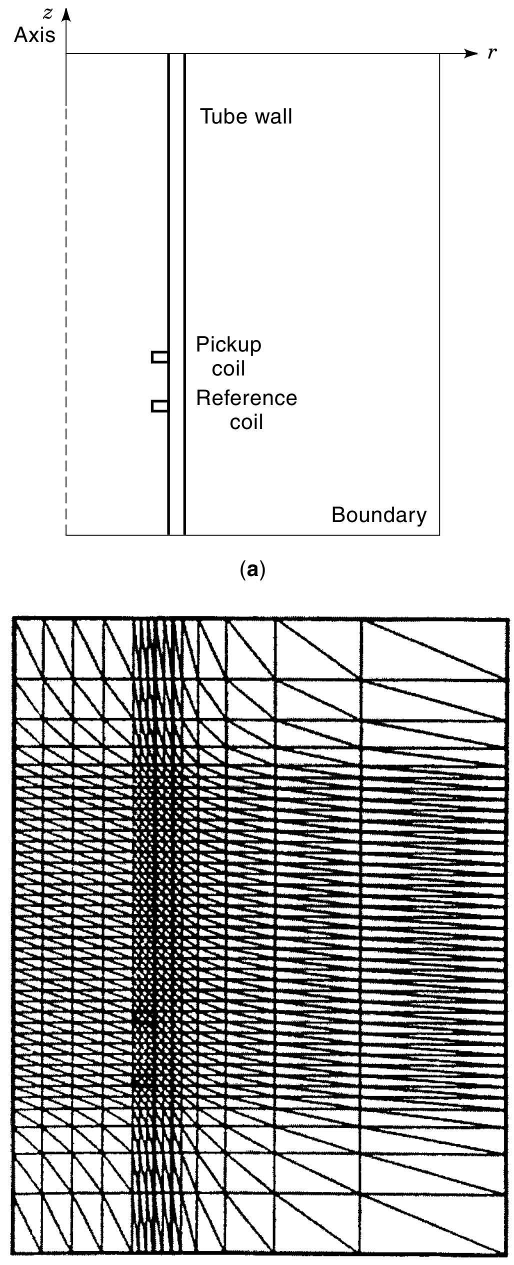

Figure 11. (a) Two-dimensional region in the axisymmetric geometry; (b) FE mesh of the region in (a).

in three unknowns A_i, A_j, A_k. These individual element equations are combined into a single global matrix equation

$$\begin{bmatrix} \ddots & & \\ & \ddots & \\ & & \ddots \end{bmatrix}\begin{Bmatrix}A_1\\A_2\\\vdots\\A_M\end{Bmatrix}=\begin{Bmatrix}Q_1\\Q_2\\\vdots\\Q_M\end{Bmatrix} \tag{37}$$

Due to the banded, symmetric, and sparse nature of the matrix, direct inversion techniques such as the Gaussian elimination method can be used to solve for the unknown vector magnetic potentials at the nodal points in the mesh.

Calculation of Eddy Current Probe Impedance

In eddy current NDT, the physical quantity that is usually measured is the impedance of the probe. The eddy current probe impedance is derived from nodal values of magnetic vector potential. The impedance Z of a single-turn coil of radius r carrying an alternating current of I_s amperes is

$$Z = \frac{V}{I_s} \tag{38}$$

where V is the phasor voltage across the coil,

$$V = -\oint_c \boldsymbol{E} \cdot \boldsymbol{dl} \tag{39}$$

Using the Maxwell–Faraday law in terms of the vector magnetic potential, $\boldsymbol{E}$ can be expressed as

$$\boldsymbol{E} = \frac{-\partial \boldsymbol{A}}{\partial t} - \nabla\phi \tag{40}$$

which for sinusoidal excitation reduces to

$$\boldsymbol{E} = -j\omega\boldsymbol{A} - \nabla\phi \tag{41}$$

Since the induced voltage is independent of the scalar potential, Eq. (41) can be substituted in Eq. (39) to get

$$\boldsymbol{E} = -j\omega \oint_c \boldsymbol{A} \cdot \boldsymbol{dl} \tag{42}$$

The impedance of the coil is

$$Z = -\frac{j\omega}{I_s} \oint_c \boldsymbol{A} \cdot \boldsymbol{dl} \tag{43}$$

which for a single-turn coil is

$$Z = j\frac{2\pi r\omega A}{I_s} \tag{44}$$

Model predicted eddy current differential probe signals for both outside-diameter and inside-diameter defects in a steam generator tube compare very well with experimental measurements (20).

The finite-element method is a very powerful tool for analyzing nonlinear, inhomogeneous boundary-value problems. Nonlinearities and inhomogeneous material properties can be incorporated very simply by specifying the material constants appropriately in each element of the discretized domain. A major advantage of the finite-element technique is that irregularly shaped boundaries can be handled easily. It is therefore ideally suited for modeling NDT problems. The boundary conditions are introduced naturally in the process of formulation of the model. Also, since the nodes do not have to be equally spaced, the mesh density can be varied depending on the field gradient in a subdomain, resulting in computational efficiencies. Finally, the implementation is relatively simple and since the matrices involved in finite-element models are sparse, banded, symmetric and diagonally dominant, the inversion process is numerically stable and robust.

The finite-element eddy current model has been extended to simulate the pulsed eddy current phenomenon (25). In this method, the spatial solution of the conventional eddy current model is combined with a finite-difference formulation in the time domain to calculate the transient solution. The model is capable of simulating the diffusion of fields into the test sample, spatial broadening of the eddy current pulse, and a propagation delay time that is proportional to the distance traveled.

EDDY CURRENT INVERSE PROBLEM

The final goal of a nondestructive test is to solve the inverse problem. The complete solution to the inverse problem involves full reconstruction of defect profiles from the sensor measurements. In eddy current testing, the physical process associated with eddy current phenomenon is diffusive in nature. This renders the task of solving the inverse problem relatively difficult. The intractable nature of the inverse problem in eddy current nondestructive evaluation (NDE) has led to the development of several engineering approaches to address the issue. One of the earliest and most widely used approaches is the calibration method, in which features associated with the measured data are compared to those derived from a set of standard signals obtained from known defects. Calibration plots for eddy current probe signals were obtained by Auld et al. (26) in which features derived from an absolute coil probe signal are directly related to defect parameters. For instance, when the flaw dimensions are larger than the coil diameter, the signal exhibits distinct "shoulders" that can be mapped to edges of the defects. The calibration plot using the features in the signal for different defect widths and theoretical inversion charts using magnitude and phase of the signal to predict defect depths are also given in Ref. 26. These procedures characterize defects in terms of an equivalent depth, width, and angle or equivalent volume. It must be mentioned that calibration methods are useful only when the defect shapes are known a priori. The method becomes invalid if the defect shapes are substantially different from the shapes of the calibration defects.

With increasing availability of greater computing resources, more sophisticated approaches to numerical inversion algorithms have been developed. These algorithms can be categorized broadly either as phenomenological or model-based and nonphenomenological or signal-classification-based methods, based on the strategy used to arrive at the inverse solution. Phenomenological models are constructed on the basis of the underlying physical process. In contrast, signal classification methods use changes in the signal features to determine the defect class. A taxonomy of inverse problem solution methods in NDE is described in Fig. 12 and an overview of some of the key work in these classes is described.

MODEL-BASED METHODS

In this section, three representative model-based approaches are discussed for finding the inverse-problem solution in terms of the defect profile in a test object. The first method is based on a volume integral formulation. The second approach

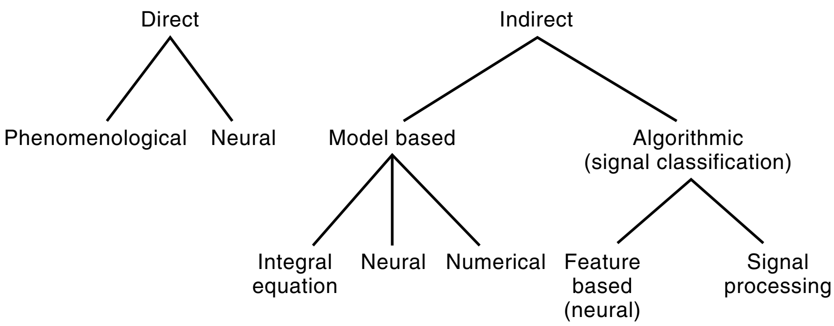

Figure 12. Taxonomy of inverse-problem solution methods.

uses an error minimization approach that involves the use of a neural network for minimizing the quadratic error function. The third approach uses a finite element forward model in an iterative scheme to determine the defect profile.

Volume Integral Approach

This technique belongs to the category of direct approaches for the inverse-problem solution. A seminumerical approach proposed by Sabbagh et al. (15) uses an analytical formulation based on the Green's function where the inverse problem is reduced to solving an integral equation of the type

$$f(r) = \int_{\Omega} G(r, r')g(r')\, d\gamma' \tag{45}$$

for the source $g(r')$ from measurements $f(r)$, where the kernel $G(r, r')$ is the Green's function. For instance, in eddy current NDE, the volume integral equation for the electric field $\boldsymbol{E}$ is

$$\boldsymbol{E}(r) = \int_{\Omega} G(r, r')\boldsymbol{J}_S(r')\, dr' \tag{46}$$

A flaw of conductivity $\sigma_f(r)$ is modeled in a host material of conductivity $\sigma_h(r)$ by an equivalent current source

$$\boldsymbol{J}_S(r) = [\sigma_f(r) - \sigma_h(r)]\boldsymbol{E}(r) \tag{47}$$

The integral equation for the perturbation field $E_p(r)$ due to the presence of the flaw is

$$\boldsymbol{E}_p(r) = \int_{\Omega_f} G(r, r')[\sigma_f(r) - \sigma_h(r)]\boldsymbol{E}(r')\, dv' \tag{48}$$

The discretization and the numerical solution of the resulting matrix give a solution of the inverse problem in terms of the conductivity profile $\sigma(r)$ of the test specimen.

Hopfield Network Approach

A novel strategy for solving Fredholm integral equations using the Hopfield neural networks was proposed by Elshafiey et al. (27). The major advantage of this method is the stability of the solution procedure that comes from the high degree of parallelism and interconnectivity used in the Hopfield network architecture.

In this algorithm, the integral in Eq. (45) is discretized using a basis-function expansion as

$$g(r) = \sum_{i=1}^{n} v_i R_i(r) \tag{49}$$

where $\{v_i\}$ are the expansion coefficients and R_i is a basis function, chosen to be a sine or cosine function. The integral equation is then written in matrix form as

$$FV = m + \eta \tag{50}$$

where $F_{ij} = \int_a^b G(r, r')R_i(r')dr'$, $m_i = f(r_i)$, $i = 1, 2, \ldots, n$ are the discrete measurements, and η represents measurement noise.

The solution vector $V = (v_1, v_2, \ldots, v_n)$ is obtained by minimizing the cost function E written in matrix form

$$\begin{aligned} E &= \tfrac{1}{2}(FV - m)^{\mathrm{T}}(FV - m) + \lambda V^{\mathrm{T}} DV \\ &\quad + \lambda_1(\Psi V - z_p)^{\mathrm{T}}(\Psi V - z_p) \end{aligned} \tag{51}$$

The first term in the cost function is the model error, the second term is a smoothness constraint included for regularization, and the third term represents the boundary conditions. Ψ is a matrix whose elements are basis functions, z_p is the system state at a given node p, and λ and λ_1 are Lagrange multipliers.

By comparing the error function in Eq. (51) to the energy function of the Hopfield neural network expressed in a similar quadratic form, the circuit parameters of the network are estimated. The network is then simulated for obtaining the solution to the integral equation. Once the Hopfield network converges to the solution vector $\boldsymbol{v}^* = (v_1^*, (v_2^*, \ldots, v_n^*)$, the defect profile can be computed using Eq. (49). The two methods just described are based on the solution of the integral equation, which, in turn, relies on the availability of the Green's function for the problem. Very often in many NDE test geometries, the computation of Green's function poses a serious challenge, limiting the applicability of the method.

An alternate scheme for eddy current inversion that overcomes this difficulty is to use the finite-element model (FEM) in the iterative scheme shown Fig. 13. In this technique, the defect is parametrized in terms of the depth coordinates at different points in the flaw region and the solution minimizes the mean-square error between the measured signal and model prediction (28).

Figure 13 outlines the procedure employed for solving the inverse problem. The iterative process starts by selecting an initial mesh configuration. The mesh coordinates are then updated until the signal predicted by the finite-element model matches the measured signal in the least-squares sense. Specifically, the coordinates of the defect profile are defined by a vector $D = (d_1, d_2, \ldots, d_n)$, which represents the depth values of the defect profile at each position on the defect boundary. The elements above and below the defect boundary are com-

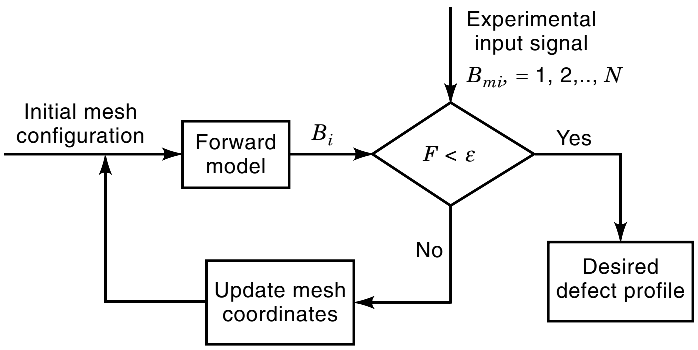

Figure 13. Schematic representation of the solution to the inverse problem.

pressed or expanded accordingly. By altering the mesh coordinates, rather than the material properties of the elements, derivatives of the unknown material property values do not have to be taken into account explicitly.

The optimal values of D are determined by minimizing an objective function of the summed square error evaluated at N measurement points:

$$F(D) = \sum_{i=1}^{N} (Z_i - Z_{mi})^2 \tag{52}$$

where Z_i ($i = 1, . . ., N$) is the calculated coil impedance using the FE method and Z_{mi} ($i = 1, . . ., N$) is the measured eddy current signal.

The error function defined by Eq. (52) is minimized using the sequential quadratic programming (SQP) approach (29). This well-known optimization procedure employs gradient information, which is derived analytically to establish the search direction. Changes in defect geometry are mapped onto a change of stiffness matrix K. The corresponding change in the source vector S is also automatically taken into account.

Model-based methods are, in general, computation intensive and are capable of determining the defect profiles only if the solution space is constrained to a suitable subspace. A different class of inversion techniques that is widely used in practice is the nonphenomenological or signal-classification approach.

SIGNAL-CLASSIFICATION METHODS

In this class of techniques, the continuum of solutions to the inverse problem is quantized into a finite number of known classes of sources or defects. These sources may represent defect classes or benign geometrical sources that also produce an eddy current signal. Examples of the latter class are the eddy current signals from edges or support-plate signals obtained in the inspection of steam-generator tubes in nuclear power plants.

A characteristic feature of all signal-classification or pattern-recognition methods is that they rely on the ability to create a data bank of all expected defect types and the corresponding signatures. This collection of signals is referred to as the training database, which is then used for training an automatic signal-classification algorithm. The classification techniques that have received a lot of attention in this area are (1) matched filters and (2) feature-based pattern-recognition methods.

Matched Filters

The matched filter (30) is a linear filter the transfer function of which is matched to a particular input signal, achieved by selecting the impulse response $h(t)$ of the filter as a reversed, shifted and scaled version of the signal $s(t)$ to which it is matched:

$$h(t) = ks(t_0 - t) \tag{53}$$

where k and t_0 are arbitrary constants. The filter then behaves as a simple correlation detector with transfer function:

$$H(j\omega) = ke^{-j\omega t_0} S^*(j\omega) \tag{54}$$

Mucciardi and Shankar (31) use this technique for the interpretation of steam-generation inspection signals. An array of filters is built in which each one is matched to the signal from a known class of defects. An unknown signal is then automatically classified by observing the response of the filters in the array.

The matched-filter algorithm is simple and easy to implement but is also prone to errors in case of any fluctuations in probe speed. Also, this procedure requires that the entire signal be stored in contrast to feature-based signal-classification methods that store and use only distinguishing features in the signal.

Feature-Based Methods

Feature-based methods form the core of automated signal-classification systems that are becoming increasingly popular in many commercial applications. An overall schematic of this approach is shown in Fig. 14.

The approach consists of two steps:

1. The first step is feature extraction, from which characteristic features in the signal that carry discriminatory information are extracted.
2. The second step is classification of the feature vector via a clustering algorithm or a neural network.

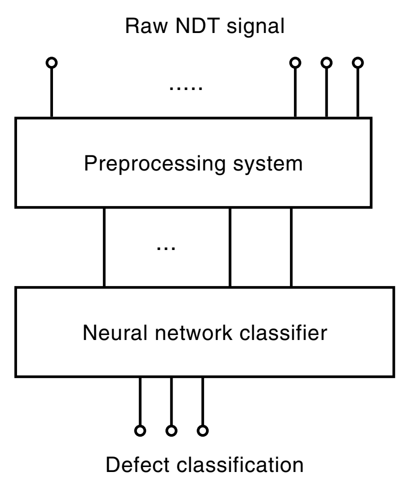

Figure 14. Schematic of the overall signal-classification procedure.

Feature Extraction. Feature extraction serves two major functions, namely, data compression and invariance processing. The vector of signal features referred to as the feature vector is extracted from a typically oversampled set of measurements. The feature extraction procedure is designed to eliminate the redundancy in the impedance plane trajectories. The entire signal is thus represented by a feature vector. The features are evaluated in the second step, called feature reduction, in which the goal is to identify those features containing the most amount of discriminatory information, in order to reduce the dimensions of the feature vector (32). One of the earlier methods used for feature reduction is the adaptive learning network, in which a polynomial representation is built from quadratic elements that use pairwise combinations of the features. The discriminatory performance of each polynomial fit is evaluated at each stage and only the "best" pairs are selected. The adaptive learning network was first introduced by Ivakhenko (33) and was applied for feature selection by Mucciardi and Shankar (31). An alternative method for feature reduction is the Fisher discrimant method (34), which calculates a statistical weight function for each feature as a measure of its ability to classify. The features are often picked from different domains, making it difficult to define a single quantitative measure for evaluating a figure of merit of the features. Furthermore, the time-domain features are sensitive to variations in probe speed and can consequently result in classification errors.

Parameter-Invariant Features. An example of features with invariance properties is obtained using a Fourier descriptor representation of eddy current impedance-plane trajectories. Fourier descriptors have been used for a long time for representing closed contours (35) in a variety of applications. This technique not only represents the signal by a few coefficients that are invariant under rotation, translation, and scaling of the eddy current impedance-plane trajectory, but also allows the resynthesis of the original signal from the stored coefficients. This results in data compression, and the error in the resynthesized signal can be used for a quantitative evaluation of the feature vector. The basic idea underlying the approach is to parametrize the impedance-plane trajectory such that the representation is periodic in the transformed domain. One such function is the complex contour function (36)

$$u(l) = x(l) + jy(l) \tag{55}$$

where $x(l)$ and $y(l)$ represent the real and imaginary components of the impedance at a distance l arc length units away from an arbitrary starting point P_0. Then $u(l)$ is periodic in l with period L,

$$u(l + L) = u(l) \tag{56}$$

Here L represents the total arc length of the curve. The periodic nature of $u(l)$ allows its expansion in a Fourier series, that is,

$$u(l) = \sum_{n=-\infty}^{\infty} c_n e^{j(2\pi/L)nl} \tag{57}$$

where

$$c_n = \frac{1}{L}\int_0^L u(l)\exp\left(\frac{-j2\pi nl}{L}\right) dl \tag{58}$$

In order to obtain descriptors of the curve that are insensitive to drift and gain setting of the eddy current instrument, the coefficients in Eq. (58) are used to compute the descriptors

$$d_n = \frac{c_{l+n}c_{l-n}}{|c_1|^2} \tag{59}$$

The descriptors d_n, $n = 1, 2, \ldots, N$ are insensitive to rotation, translation, and scaling of the curve. The implication of this invariance is that changes in the signal due to the instrument gain drift or gain settings will not affect the interpretation of the signal. The parametric representation $u(l)$ also ensures that variations in probe speed will not affect the final result.

The two procedures for feature extraction described previously illustrate the use of appropriate signal features for achieving data compression and invariance to selected experimental parameters. A K-means clustering or a neural network is used to classify the feature vector.

Classification Algorithms

The second step in signal-classification systems is the labeling of the feature vector. Two of the widely used techniques for classifying eddy current signals are (1) clustering algorithms and (2) neural networks.

***K*-Means Clustering.** In a clustering algorithm, a feature vector of length n is treated as a point in an n-dimensional feature space. The set of feature vectors from a similar class of signals are expected to cluster together in the feature space. Clustering algorithms are capable of identifying the clusters in either a supervised (with training data) or unsupervised (without training data) mode. The K-means algorithm (34) partitions the set of feature vectors into K disjoint subsets such that a performance index is minimized. The performance index is typically chosen to be the sum of the squared Euclidean distances between a cluster center and all the points contained within that cluster. The algorithm is iterative in nature and during each cycle the cluster centers are updated. The performance of the algorithm can be improved significantly if the K cluster centers during the first iteration are drawn from K different classes of signals in the training data.

Neural Networks. Neural networks represent an attempt to mimic the biological nervous system with respect to both architecture as well as information-processing strategies (37). These networks consist of simple processing elements that are interconnected via weights. The network is first trained using training data and an appropriate learning algorithm for the estimation of the interconnection weights. Once the network is trained, unknown test signals can be classified. The class of neural networks used most often for classification

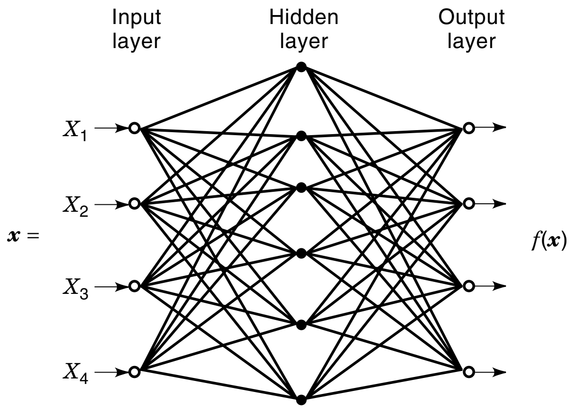

Figure 15. Multilayer perceptron neural network.

tasks is the multilayer perceptron (MLP) network (37) shown in Fig. 15.

The multilayer perceptron network generally consists of an input layer of nodes, one or more hidden layers of nodes, and an output layer of nodes. The nodes within the same layer are not connected but each layer of nodes are fully interconnected to the nodes in the next layer. All units within a layer process data in parallel, but the outputs of different layers are calculated sequentially starting from the input layer and moving towards the output layer. Each node j in a layer $k + 1$ performs the following computations.

Step 1. The input to node j, x_j, is

$$x_j = \sum_{i=1}^{N_k} w_{ij} y_i \tag{60}$$

where y_i is the output of node i in layer k, N_k is the number of nodes in layer k, and w_{ij} are the interconnection weights.

Step 2. The output of node j, y_j, is

$$y_j = f(x_j) = \frac{1}{1 + \exp[-(x_j + \theta_j)]} \tag{61}$$

where θ_j is a bias variable. This nonlinear function is primarily used to limit the output of a node between the values of 0 and 1.

One of the most commonly used training algorithms is the backward error propagation algorithm (38) in which training patterns are sequentially applied to the network. The algorithm uses a gradient search technique for minimizing the squared error between the actual output and the desired output by iteratively adapting the interconnection weights. The algorithm cycles through the training data until the error drops below a specified threshold value. Neural networks have been used with considerable success in the classification of eddy current and ultrasonic NDE signals (39,40). These networks are also capable of learning in an incremental mode and use prior knowledge for improving its performance with time.

PULSED EDDY CURRENT SIGNAL PROCESSING

The processing of pulsed eddy current signals for defect characterization is based on a calibration approach where the features are peak amplitude and zero crossover point of the waveform (41). The peak amplitude is proportional to the amount of metal loss and the zero crossover point, which is proportional to the propagation time, carries information about the depth of the flaw. Time gated images of the peak voltage, called C-scan images, provide information relating to material properties at different depths within the sample. The pulsed eddy current technique has proved to be particularly advantageous in the inspection of multilayer structures encountered in the aerospace industry.

BIBLIOGRAPHY

1. D. J. Hagemaier, *Fundamentals of Eddy Current Testing,* Columbus, OH: American Society for Nondestructive Testing, 1990.
2. R. Halmshaw, *Non-destructive Testing,* London: Edwin Arnold, 1991.
3. J. D. Jackson, *Classical Electrodynamics,* New York: Wiley, 1975.
4. V. S. Cecco, *Eddy Current Manual,* Ontario: Chalk River National Laboratories, 1983.
5. S. Sharma et al., Finite Element Modeling of Eddy Current Probes for Edge Effect Reduction, in D. O. Thopmson and D. E. Chimenti (eds.), *Review of Progress in Quantitative Nondestructive Evaluation,* New York: Plenum, 1997, vol. 16A, pp. 201–208.
6. W. Podney and J. Moulder, Electromagnetic Microscope for Deep, Pulsed, Eddy Current Inspections, in D. O. Thompson and D. E. Chimenti, (eds.), *Review of Progress in Quantitative Nondestructive Evaluation,* New York: Plenum, 1997, vol. 16A, pp. 1037–1044.
7. S. D. Brown, Multifrequency/Multiparameter Eddy Current Steam Generator NDE, in R. B. Clough (ed.), *Quantitative NDE in the Nuclear Industry,* Metals Park, OH: ASM, 1983.
8. J. Stolte, L. Udpa, and W. Lord, Multifrequency Eddy Current Testing of Steam Generator Tubes using Optimal Affine Transform, in D. O. Thompson and D. E. Chimenti (eds.), *Review of Progress in Quantitative Nondestructive Evaluation,* New York: Plenum, 1988, vol. 7A, pp. 821–830.
9. T. R. Schmidt, The remote field eddy current inspection technique, *Mater. Eval.,* **42**: 225–230, 1984.
10. W. Lord et al., A finite element study of the remote field eddy current phenomenon, *IEEE Trans. Magn.,* **24**: 435–438, 1988.
11. J. L. Fisher and R. E. Beissner, Pulsed Eddy Current Crack Characterization Experiments, in D. O. Thompson and D. E. Chimenti (eds.), *Review of Progress in Quantitative Nondestructive Evaluation,* New York: Plenum, 1986, vol. 5A, pp. 199–206.
12. Avanindra, *Multifrequency eddy current signal analysis,* M.S. Thesis, Iowa State University, Ames, IA, 1997.
13. C. V. Dodd and W. E. Deeds, Analytical solutions to eddy current probe coil problems, *J. Appl. Phys.,* **39** (6): 2829–2938, 1968.
14. B. A. Auld, F. Muennemann, and M. Riaziat, Quantitative modeling of flaw and responses in Eddy Current Testing, in R. S. Sharpe (ed.), *Research Techniques in Nondestructive Testing,* New York: Academic Press, 1984, vol. 7.
15. H. A. Sabbagh and D. L. Sabbagh, *Development of a System to Invert Eddy Current Data and Reconstruct Flaws,* Final Report, Contract No. N60921-81-C-0302 with Naval Surface Weapons Center Code R34, White Oaks Laboratories, June, 1982.

16. P. E. Wannamaker et al., Electromagnetic modeling of three dimensional bodies in layered earths using integral equations, *Geophysics,* **49** (1): 60–74, 1984.

17. C. V. Dodd, *Solutions to electromagetic induction problems,* Ph.D. Dissertation, Univ. Tennessee, Knoxville, 1967.

18. M. V. Chari, Finite element solution of the eddy current problem in magnetic structures, *IEEE Trans. Power Appar. Syst.,* **PAS-93**: 62–72, 1974.

19. J. R. Brauer, Finite element analysis of electromagnetic induction in transformers, presented at the *IEEE Winter Power Meet.,* New York, January, 1977.

20. R. Palanisamy and W. Lord, Finite element analysis of eddy current phenomena, *Mater. Eval.,* **38** (10): 39–43, 1980.

21. R. Palanisamy and W. Lord, Finite element analysis of axisymmetric geometries in quantitative NDE, in *Proc. ARPA/AFML Review of Progress in Quantitative NDE,* San Diego, July 1979.

22. N. Ida, *Three dimensional finite element modeling of electromagnetic NDT phenomena,* Ph.D. Dissertation, Colorado State Univ., CO, 1983.

23. L. J. Segerlind, *Applied Finite Element Analysis,* New York: Wiley, 1976.

24. O. C. Zienkiewicz, *The Finite Element Method in Engineering Science,* London: McGraw-Hill, 1971.

25. B. Allen, *Finite element modeling of pulsed electromagnetic NDT phenomena,* M.S. Thesis, Colorado State University, CO, 1983.

26. B. A. Auld et al., Improved Prove-Flaw Interaction Modeling, Inversion Processing and Surface Roughness Clutter, in D. O. Thompson and D. E. Chimenti (eds.), *Review of Progress in Quantitative NDE,* New York: Plenum, 1984, vol. 2.

27. I. Elshafiey, L. Udpa, and S. S. Udpa, Solution of inverse problems in electromagnetics using Hopfield networks, *IEEE Trans. Magn.,* **31**: 852–861, 1995.

28. M. Yan et al., Solution of inverse problems in electromagnetic NDE using finite element methods, *IEEE Trans. Magn.,* **34**: September 1998.

29. K. Shittkowski, On the convergence of a sequential quadratic programming method with an augmented lagnangian line search functions, in *Series Optimization,* Mathematische Operationsforschung und Statistik, vol. 14, 1983.

30. G. L. Turin, An introduction to matched filters, *IRE Trans. Inf. Theory,* **IT-6**: 311–329, 1960.

31. A. N. Mucciardi and R. Shankar, *Signal Processing for ISI,* EPRI NP-121, Sec. 4, May 1980.

32. P. A. Doctor et al., Pattern Recognition Methods for Classifying and Sizing Eddy Current Using Eddy Current Data, in G. Birnbaum and G. Free (eds.), *Eddy Current Characterization of Materials and Structures,* ASTM STP 722(ASNT), Philadelphia: ASTM, 1981.

33. A. G. Ivakhenko, The group method of data handling—A revival of the method of stochastic approximation, *Sov. Autom. Control,* **13** (3): 43–55, 1968.

34. J. T. Tou and R. C. Gonzales, *Pattern Recognition Principles,* Reading, MA: Addison-Wesley, 1974.

35. E. Persoon and K. S. Fu, Shape discrimination using Fourier descriptors, *IEEE Trans. Syst. Man Cybern.,* **SMC-7**: 170–179, 1977.

36. C. T. Zahn and R. Z. Roskies, Fourier descriptors for plane closed curves, *IEEE Trans. Comput.,* **C-21**: 269–281, 1972.

37. R. P. Lippman, An introduction to computing with neural nets, *IEEE ASSP Mag.,* **4** (2): 4–21, 1987.

38. D. E. Rumelhart, G. E. Hinton, and R. J. Williams, Learning Internal Representations by Error Propagation, in D. E. Rumelhart and J. L. McClelland (eds.), *Parallel Distributed Processing: Exploration in the Microstructure of Cognition,* Cambridge, MA: MIT Press, 1986.

39. L. Udpa and S. S. Udpa, Eddy current defect characterization using neural networks, *Mater. Eval.,* **48** (3): 342–347, 1990.

40. J. Chao, L. Udpa, and S. S. Udpa, Ultrasonic Signal Analysis Using Wavelet Transform, in D. O. Thompson and D. E. Chimenti (eds.), *Review of Progress in Quantitative Nondestructive Evaluation,* New York: Plenum, 1993, pp. 735–742.

41. J. A. Bieber et al., Time-Gating of Pulsed Eddy Current Signals for Defect Characterization and Discrimination in Aircraft Lap-Joints, in D. O. Thompson and D. E. Chimenti (eds.), *Review of Progress in Quantitative Nondestructive Evaluation,* New York: Plenum, 1997, vol. 16, pp. 1915–1921.

Satish S. Udpa
Lalita Udpa
Iowa State University